Cold Regions Science and Technology 213 (2023) 103912

Contents lists available at ScienceDirect

Cold Regions Science and Technology

journal homepage: www.elsevier.com/locate/coldregions

Experimental rig for ice accretion and adhesion strength measurement for air cycle machine system

A. Vincent [a,*], M.L.A. Pervier [a], H. Pervier [a], D. Nalianda [a], P. West [a], C. Agustin-Saenz [b], F. Brusciotti [b]

[a] School of Aerospace, Transport and Manufacturing, Cranfield University, College Road, MK43 0AL, UK
[b] TECNALIA, Basque Research and Technology Alliance (BRTA), Mikeletegi Pasealekua 2, 20009 Donostia - San Sebastian, Spain

ARTICLE INFO

Keywords:
Ice accretion
Ice adhesion
Ice protection
Air cycle machine
Shear test
Icephobic coating

ABSTRACT

Air cycle machines (ACM) which are part of the air-conditioning pack in every aircraft, are one such turbomachinery device that can be affected by icing issues particularly at the turbine end. Current ice protection solutions for the air cycle machines use a heating system on the downstream pipe to heat the surface, using electric resistance heaters or hot air coming from the ACM compressor stage. Both solutions require high energy, hence the need to reduce energy consumption through the development of passive energy-saving solutions.

Clean Sky 2 ERICE project aims at developing an eco-friendly and cost-effective hydrophobic / ice-phobic solution able to resist ice adhesion in the ACM turbine scroll and its downstream pipe. This paper discusses the implementation of an experimental rig to reproduce the ice formation and accretion conditions within the ACM and a new shear test method to measure the ice adhesion strength on existing and new solutions in the form of coatings. The flow through the ACM turbine exhaust has also been characterized for the first time in published literature. The results from the ice accretion and adhesion tests show that hydrophobic coatings developed for the purposes of ice protection perform better than the current industry baseline material for ACM turbine scroll pipe internal surface. While these coatings could not be used to prevent accretion, they do help in reducing adhesion of ice to the surface.

1. Introduction

Icing is considered a serious challenge within aviation with a lot of research focused on de-icing and anti-icing systems. Accretion of ice on aircraft surfaces or within aircraft systems operating at high altitudes or humid conditions is a common occurrence and poses a safety threat which needs to be countered regularly for a safe flight (SD, 2006). The build-up of ice on these systems can occur during any phase of the flight – taxi, take-off, climb or cruise etc. Apart from aircrafts, ice build-up can be dangerous in infrastructure, oil rigs, solar panels, wind turbines, transmission lines etc. (Andenæs et al., 2018; Ryerson, 2011; Gao and Hu, 2021). Thus, effective solutions to prevent accretion of ice or reduce the ice adhesion strength on the structure so that it can be removed with ease, is of great importance. Ice protection has been an area which has been under constant focus for many industries including aerospace and has long warranted application of more green and eco-friendly technologies. The current anti-icing and de-icing systems can be classified as "active systems" which consume energy in exchange for providing safe, ice-free surfaces or systems. The new push within most mechanical and civil industries, but mainly within aerospace, is towards more greener technologies (Clean Sky 2, 2015). This means for aircraft ice protection systems the need to focus on more passive solutions which consume less energy, help in structural or system weight reduction thereby improving the specific fuel consumption (SFC).

The paper describes an experimental rig, built to reproduce the ice accretion conditions within an air cycle machine (ACM) turbine scroll pipe and a new shear adhesion test technique that measures the adhesion strength of the accreted ice in the scroll pipe sample. Various coatings, commercial and custom-built for ice protection applications, have been tested as samples for this research along with the current baseline material. The coatings are hydrophobic in nature designed to have very low surface free energy. Additional tests have been carried out to characterize the flow, determine the droplet size and simulate the ice protection hot lip system present in the ACM by the means of a trace-

* Corresponding author.
E-mail address: abhay.vincent@cranfield.ac.uk (A. Vincent).

https://doi.org/10.1016/j.coldregions.2023.103912
Received 21 January 2023; Received in revised form 26 April 2023; Accepted 25 May 2023
Available online 2 June 2023
0165-232X/© 2023 The Authors. Published by Elsevier B.V. This is an open access article under the CC BY license (http://creativecommons.org/licenses/by/4.0/).

wire setup. The results from the tests have been reported along with the conclusions.

2. Research background

2.1. Air cycle machine system

The ACM is a turbomachine device which is part of the Environmental Conditioning System (ECS) (Boeing Commercial Aircrafts, 2011). In the most commonly used configuration, the ACM is a single-stage, one spool, compressor-turbine arrangement which is used for cooling down the hot air bleed that is received by the ECS system from the compressor stage of the aircraft engine.

2.2. Icing issues in ACM turbine and downstream pipe

Icing issues are an important design parameter in air cycle machines used in the aircraft especially at the turbine end. Typically, the air cycle machines use a heating system on the downstream pipe called de-icing ring to heat the surface of the pipe. The temperature source can be from electric resistance heaters or hot bleed air. However, those two solutions are energy consuming, and the current need is to reduce energy consumption through the development of passive energy-saving solutions.

The turbine exhaust of the ACM experiences very low temperatures due to the expansion of the air and thus the pipe immediately downstream of the turbine in some configurations can see the build-up of ice – this has been observed mostly in hot weather conditions when the moisture levels in the air is high. This necessitates the use of an active ice protection system that takes bleed air from the compressor exit of the ACM and feeds a 'heated lip' on the downstream pipe. This prevents the accretion of ice in the pipe walls. The ice protection system, however, greatly reduces the efficiency of the ACM system by extracting the hot bleed air from the compressor to power the heated lip. This results in high energy consumption which isn't ideal and leads to the need of developing a passive ice protection system for the future.

This has led to the icing issue to be of major interest to ACM manufacturers who want to develop a more efficient and eco-friendly system that can perform in accordance with the objectives laid down by Clean Sky 2 (Clean Sky 2, 2015). This is where superhydrophobic and icephobic coatings have come into the picture. In simple terms, superhydrophobic coatings are a surface layer that repels water and in general have a contact angle equal or $>150^0$ and hysteresis of water contact angle below 10° (Kulinich et al., 2009; Jung et al., 2012). Icephobic coatings on the other hand, delay ice nucleation and significantly reduce ice adhesion (Kool et al., 2018; Laforte et al., 2015). Covering the airframe structures and engine systems with such coatings can help in resisting the build-up/accretion of ice or ease its removal by reducing the ice adhesive strength to the structure (Beeram et al., 2017). This in turn would reduce the amount of bleed extracted from the hot-air sources like the aircraft engine / ACM thereby improving the overall efficiency of the system, reducing weight and the Specific Fuel Consumption (SFC). Thus, a lot of research in the area of ice protection systems in aerospace has been focussed in recent years on the development of superhydrophobic and icephobic coatings.

3. Experimental test setup and procedure

3.1. Icing rig design and construction

The aim of the rig presented below was to recreate the ice accretion process encountered in the downstream pipe of an ACM. The ice produced in an ACM is due to the freezing process of moisture after expansion of the air through a turbine. Therefore, instead of using an icing wind tunnel or a cold room as usually the case for icing experiments, a standalone rig was developed. The ACM itself is replaced by a vehicle turbocharger, due to its similar work principle and ease of acquisition. The system consisted of an intake of warm dry air in which water was injected in a controlled manner before going through the turbine of the turbocharger (Fig. 1). The expansion of air through the turbine resulted in a drop of temperature leading to the formation of ice within the exhaust pipe.

The air supplied to the rig (Fig. 2) was provided by a 20-bar Ingersoll-Rand compressor at a temperature of 10–12 °C and a mass flow of 1 kg/s. The supply pressure to the rig was 4 bars.

The air supplied was sent through an air-water heat exchanger in order to raise its temperature. The maximum output dry air temperature was about 60 °C. The water supplying the air/water heat exchanger was coming from a parallel circuit comprising a water reservoir and a heater to reheat the recirculating water at each passage. The water heating device was custom-built and consisted of immersion heaters.

The hot dry air was humidified by a water injection system, positioned inside of the pipe circulating air, and producing a very fine mist. Based on a flow requirement of 0.5 kg/s and a liquid water content of 20 g/kg of dry air, the required amount of water that needs to be supplied was around 36 kg/h. The water injection system consisted of a single atomiser nozzle (size: PJ15, orifice diameter of 0.38 mm and spray angle of 90°) capable of providing droplets size between 20 and 100 μm. It was completed by a water reservoir and a water pump to supply the water at the right pressure. The amount of water injected in the rig was controlled by a flowmeter.

Post the addition of water, the pipe needed to be long enough so the water would mix effectively in the airflow. The evaporation rate for a single droplet in a freestream is given by Eq. (1):

$$\frac{dm}{dt} = Sh^*\pi^*D^*\rho c^*Dv^*(\omega A, s - \omega A,\infty) \quad (1)$$

where,

- d_m/d_t – Evaporation rate of droplet
- S_h – Sherwood Number = 21.56
- D – Droplet diameter = varied from 10 μm to 100 μm
- ρ_c – Freestream Gas Density = 1.06 kg/m^3 at 60 ^{0}c
- D_v – Diffusion coefficient of water vapour in air = 9.41 × 10^{-5} m^2/s
- $\omega_{A,s}$ – humidity of saturated air = 0.0167
- $\omega_{A,\infty}$ – humidity of surrounding air = 0.00169

Based on the calculation method elaborated in (Grosshans, 2012), the evaporation rate for the water droplets for varying relative humidities and droplet sizes was calculated. The evaporation rate is then used to determine the time taken for evaporation of a droplet in seconds. Using this time taken and an assumed freestream velocity of air in m/s, the length of the pipe was calculated in metres. The variation of the droplet size from 10 to 100 μm and the variation in relative humidity from 0 to 100% were used to define the variation in the length of the pipe and the worst-case length of 3.7 m was calculated. Adding an additional buffer, a 5-m-long pipe was used between the water injection and air expansion device. The pipe was connected to the turbine inlet of a Holset HX-35 turbocharger through which the humid, compressed air was expanded.

3.1.1. Rig instrumentation and data acquisition setup

A National Instruments (NI) Data Acquisition System (DAQ) was used for acquisition of signals from all types of sensors – Pressure, Thermocouples, Mass Flow (Orifice Plate), Mass Flow (Water System) as summarized in Fig. 3. A video Camera was installed facing the exhaust of the turbocharger to observe the ice accretion on the exhaust pipe and the turbine blades. It was connected to the control room PC screen and recording was taking place via the Open Broadcasting Software (OBS). Infrared or IR mode was selected for clear view and avoiding any exposure difficulties. A Chilled Mirror was also utilised to obtain relative

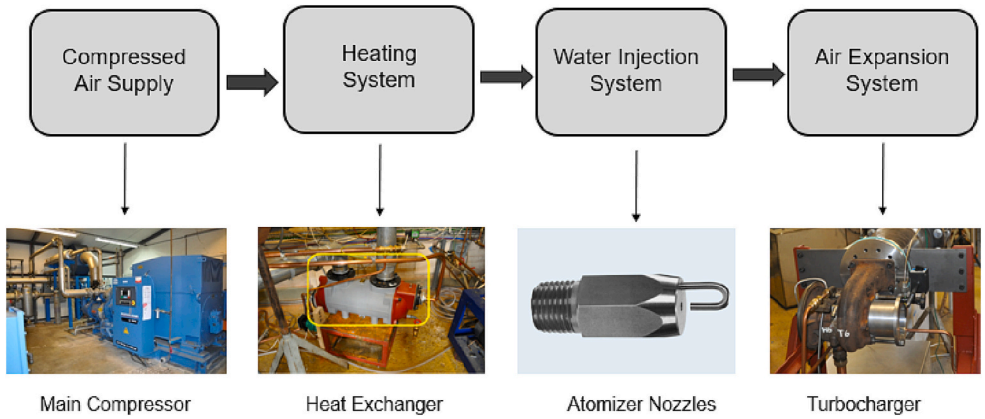

Fig. 1. Conceptual design of icing rig.

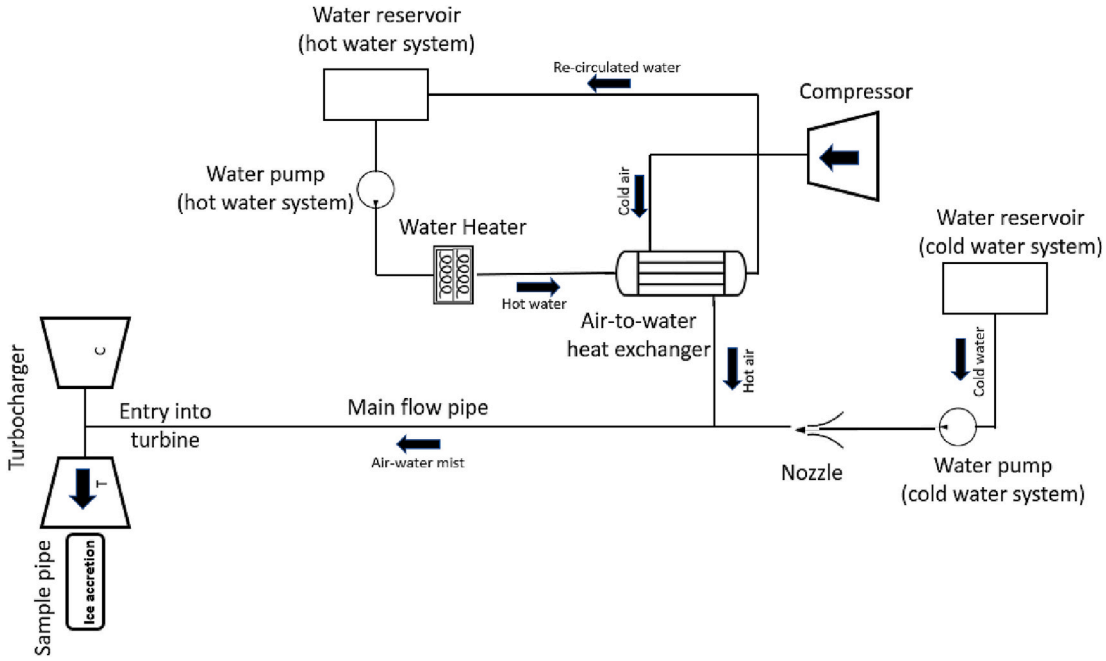

Fig. 2. Schematic of ACM icing rig.

humidity measurements at the inlet of the turbine. The chilled mirror output was relayed directly to the control room PC. In order to monitor the turbocharger, a turbine speed sensor was used which measures the Revolutions per minute (RPM) of the turbine stage during operation.

3.1.2. Scrape test design

To measure the adhesive shear strength of the ice accreted on the pipe downstream of the turbocharger, a scrape test similar to the one used in the coating industry was developed and manufactured. The aim was to delaminate the ice that has formed inside the pipe in a shear manner but without scraping the coating of the pipe.

A conceptual design of the test principle is presented on Fig. 4. Heated copper blades were used to melt the ice accreted on the pipe downstream of the turbocharger and to create grooves so a block of ice could be isolated from the rest of the ice accretion. Based on the previous experience testing (Pervier, 2012), it was determined that a 20x20mm ice block would provide enough amount of accreted ice to provide a clear adhesive break. A scrapper with a curved head was positioned against the block of ice and pushed with gradual force until delamination occurs. The force on the scrapper arm was applied by a pneumatic actuator and measured by a load cell. The design was completed by a V-clamp base, a support block and a base platform as shown in Fig. 5.

As the test needs to be performed in cold conditions so that the accreted ice does not melt, the whole test setup was placed at the bottom a − 20 °C chest freezer.

3.2. Ice protection coatings

Different types of coatings, both commercial and developed by TECNALIA (Spain) within the framework of ERICE project, were employed to be tested in the ice test rig developed at Cranfield. All coatings were applied on aluminium alloy AA2024-T3 substrate. The commercial coatings were a thin sulfuric acid anodizing (TSAA) applied on AA2024-T3 and sealed with SOCOSURF TCS-PACS or with PTFE (Teflon®), and two commercial paints, Wearlon and Xylan respectively, as detailed in Table 1.

TECNALIA (Spain) implemented an innovative solution consisting of thin coatings developed by sol-gel technique and applied by dipping on AA2024-T3. The baseline coating formulation contain a silica, hybrid and organic precursors and a zirconia or titania precursor mixed with a complexing agent. The resulting formulation was complemented with the addition of polyfluorocarbon and alkyl-alkoxy silanes in order to

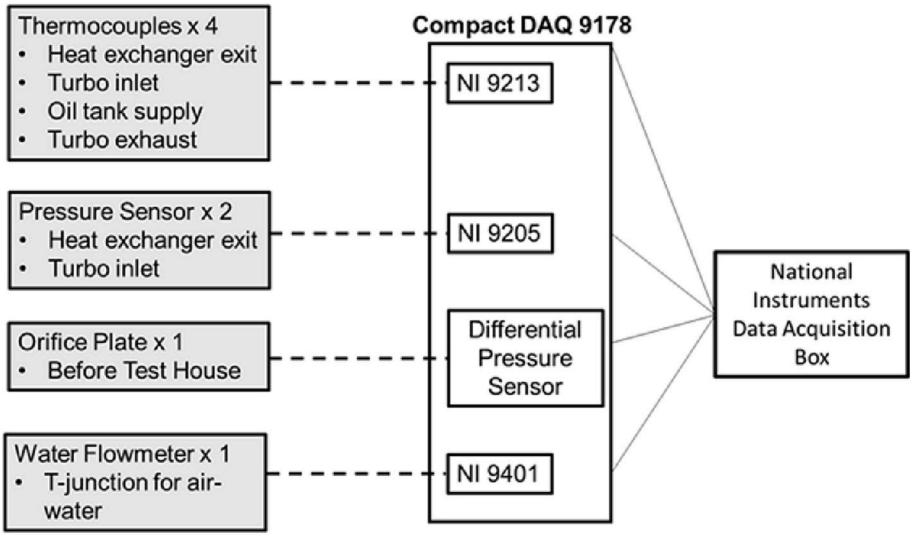

Fig. 3. Instrumentation setup for icing rig.

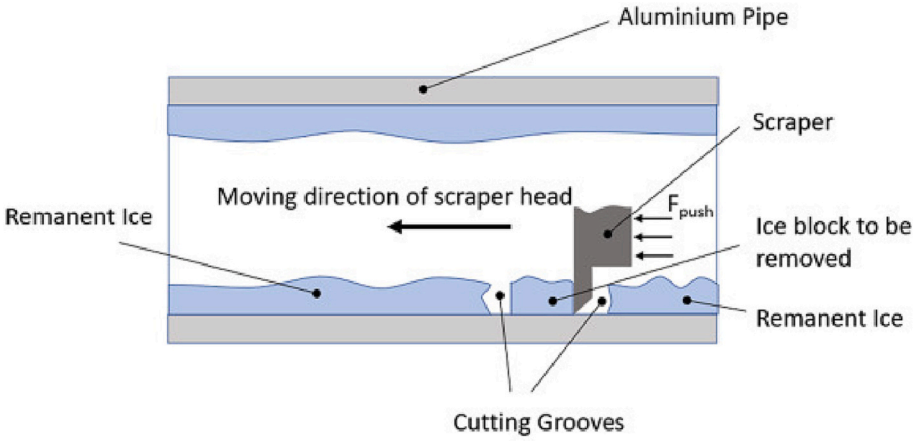

Fig. 4. Conceptual design for a scrape test for accreted ice, (An et al., 2022).

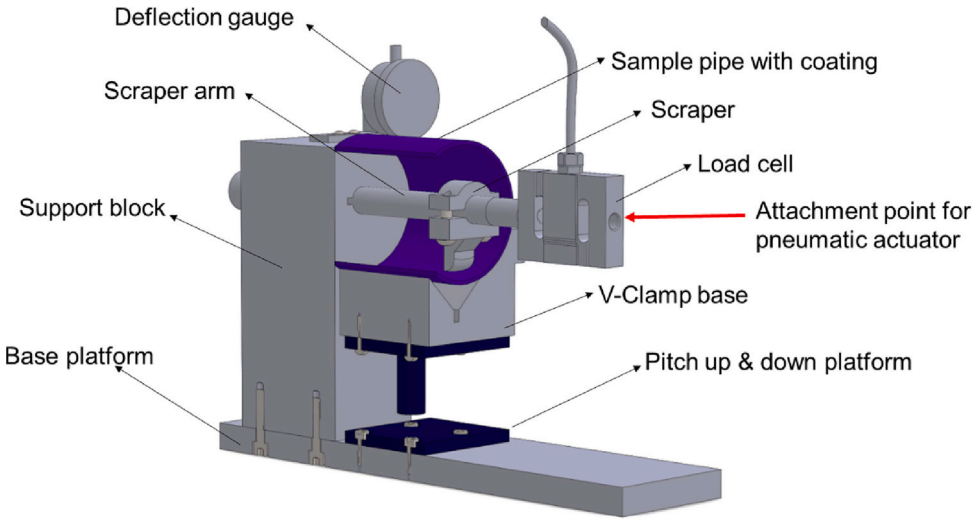

Fig. 5. Detailed design of scrape adhesion test.

Table 1
Commercial and proprietary coatings tested for ice properties.

Reference	Contact Angle (water)	Contact Angle (hexadecane)	Surface free energy (mJ/m^2)	Treatment
Thin SAA	114	7	27.4	Thin Sulfuric Acid Anodizing sealed with TCS-PACS *on AA2024-T3*
PTFE	138	30	27.4	Thin Sulfuric Acid Anodizing sealed with PTFE *on AA2024-T3*
Wearlon	102	28	25.2	Super F-6 M *on AA2024-T3, by Wearlon*
Xylan	120	31	24.3	XYLAN 1514/G7122 white aluminium *on AA2024-T3, by Whitford*
TEC-Fsmooth	105	63	16.2	Coating with high viscosity and thickness > 5 μm, *on AA2024-T3*
TEC-Fthin	105	52	19.0	Coating with low viscosity and thickness between 1 and 1.5 μm, *on AA2024-T3*
TEC-Fsmooth on TSAA	94	43	23.8	TEC-Fsmooth applied on AA2024-T3 treated with Thin SAA

obtain hydrophobic coatings.

By varying the formulation parameters, two specific coatings were optimized for low surface free energy behaviour to fulfil the requirements for corrosion and erosion resistance with ice protection performance (TEC-Fsmooth and TEC-Fthin). The two coatings were also applied on a AA2024-T3 substrate previously treated with Thin SAA sealed with TCS (TEC-Fsmooth on TSAA). Table 1 lists all the coatings tested for ice-properties.

3.3. Test procedure

3.3.1. Ice accretion

In order to accrete ice in the selected pipe sample, the latest was attached to the turbine exhaust. The rig was set to the required test condition and once stabilized in dry conditions, the water injection was started. Ice was allowed to accrete on the sample for a duration of 180 s. This duration was determined after multiple preliminary tests and set in order to keep the basis of comparison of the samples fair and consistent. It was observed that after 180 s of accretion, there was usually a 1.5-2 mm of accretion on the sample pipe which was the minimum amount of accretion necessary for the scrape test to work. After the 180 s, the operator shut the rig down and the sample pipe was moved into the freezer after it is unscrewed from the turbo exhaust. This process takes about 30 s for every run as the freezer was placed close to the rig to avoid delay in transfer. The mechanism to hold the pipe to the turbo exhaust was designed to allow a quick release. This is a crucial part of the test procedure since delay in moving the sample to the freezer can cause the sample to start melting and for the ice characteristics to change. The ice was left in the freezer for a minimum duration of 15 mins before being tested with the scrape test. Fig. 6 shows the sample pipe before and after ice accretion.

3.3.2. Scrape test

The sample once stabilized was first evaluated for ice accretion thickness around the points of maximum accretion. Multiple tests

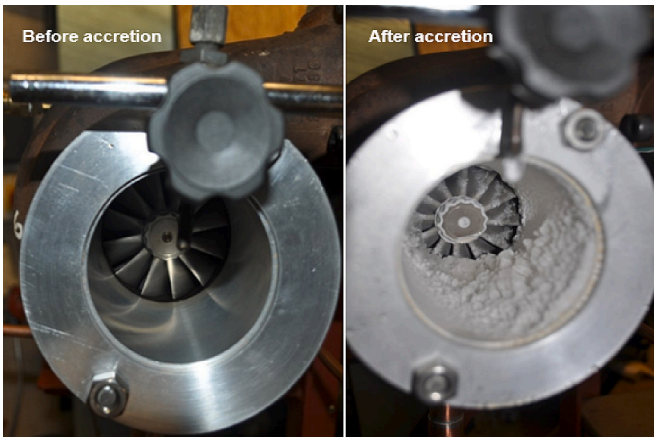

Fig. 6. Aluminium sample attached to the turbocharger exhaust (before and after ice accretion).

showed this point to be usually at the 5 o'clock position from the Top Dead Centre (TDC) of the cylindrical pipe. Once the accretion thickness was recorded, the images of the accretion within the pipe were captured using a digital single-lens reflex (DSLR) camera.

A square ice block of 20x20mm was cleared into the accreted ice in the sample around the point of maximum accretion determined previously using a heated rectangular piece of copper. Since the process of clearing the ice was done manually, it was not always perfect and could result in slightly different sizes of ice blocks. To ensure that this variance in size was accounted for in the calculation of the adhesion strength, each ice block was measured using a Vernier calliper. A path in the front and back of the ice block was cleared using a heated copper ring to ensure that the scraper blade has enough space to move freely. This was done mainly to avoid several delamination points on the force-time curve and have just one main peak force recording. The time taken for square block to be cut and the sample to be ready for the scrape test was around 5 mins per sample.

The iced pipe sample was then placed into the V-base of the test setup and its height was adjusted using a scissors lift until the scraper head was just above the surface of the pipe. The scraper head should not be touching the pipe surface to avoid any damage of the coating during the test. Once the position was set, the scraper was moved until it made slight contact with the front face of the ice block. The scraper arm was completely halted once the scraper face engages the ice face. The load cell was then fitted to the arm with the pneumatic actuator. The actuator arm was then engaged to meet the scraper arm. Once the datalogging was started, the pneumatic actuator then statically loaded the scraper arm until the ice was delaminated off the surface. The resultant force was captured with the help of the load cell. Only the values which follow fully adhesive removal were kept. During the test campaign, only 3 tests were considered as failed out of 45 total tests conducted. The mean strain rate for the test is calculated to be around 5×10^{-6} s^{-1}, which indicates the brittle mode of ice (Gold, 1970; *Trans. Can. Soc. Mech. Eng.*, 1989).

For each sample, a minimum of five scrape tests were conducted to fully assess the associated scatter and average value of the adhesion strength. Using the ice block dimension as the contact area, the adhesion strength was then calculated as per Eq. (2) (Xiao et al., 2017):

$$\tau_{adhesion} = \frac{F_{peak}}{A_{contact}} \tag{2}$$

where, $\tau_{adhesion}$ is the adhesion strength, F_{peak} is the peak force recorded for the test and $A_{contact}$ is the contact area based on ice block dimensions.

Fig. 7 shows an example of the sample with ice accreted within and post delamination of the ice block where the ice has been removed cleanly. Fig. 8 shows an example of the peak force on the force-time

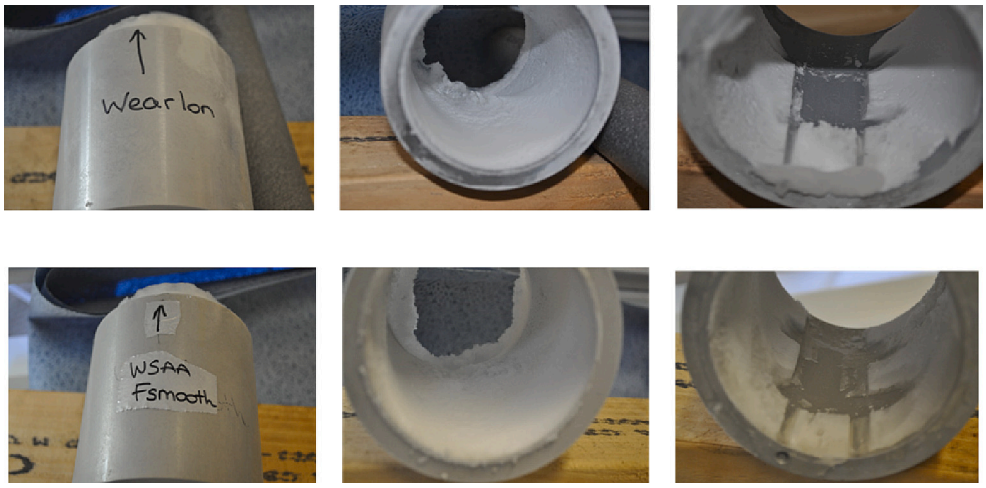

Fig. 7. Example of sample with ice accreted and post delamination.

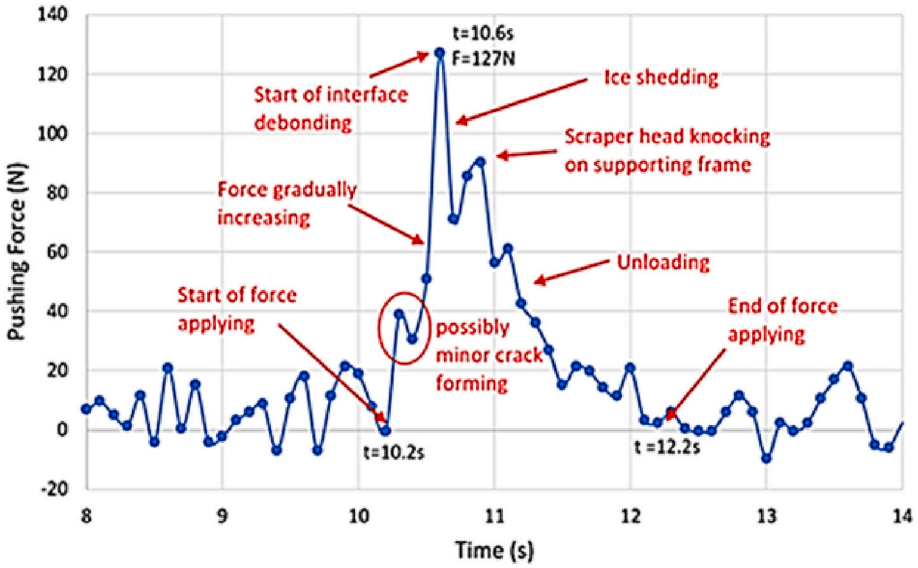

Fig. 8. Example of force-time curve.

diagram. The gradual increase of the force could easily be spotted as well as a sharp decrease at 10.6 s which indicates the delamination of ice. The force associated with the instant of delamination is referred as the peak force.

3.4. Additional tests setups

3.4.1. High speed camera setup and test process

The flow characterization was done primarily with the help of a Photron Fastcam SA4 High Speed Camera and a flashing Light Emitting Diode (LED) setup. For this test, the turbocharger exhaust was not attached with any samples and the camera and the LED were placed on opposing sides. This technique is commonly referred to as the"shadowgraphy technique". The focus of the camera was adjusted to best capture the particles at the highest possible frame-rate, as effectively and clearly as possible. The camera was set to operate at 50,000 frames per second (fps) capturing a 1.8 s video of the flow. The scale for the camera was determined to be 0.0436 mm/pixel and the LED flash duration was set at 0.5 μs.

3.4.2. Spraytec Malvern particle analyser setup and test process

The Spraytec Malvern Particle Analyser was used to characterize the flow and to ascertain various physical and flow properties of the particles in the simulated ACM icing conditions generated by the rig. The Malvern was set up and focused near to the centreline of the exhaust. This instrument, capable of measuring a wide size range of spray droplets and spray particles (0.1–2000 μm), measure intensity of light scattered as a laser beam passes through a spray. This data is then analysed to calculate the size of the droplets that created the scattering pattern. For this application, the 300 mm lens was chosen as it would cover the necessary range of droplet sizes expected within the flow (0.1–900 μm (Dv50: 0.5–600 μm)).

3.5. Trace wire heating setup

To simulate the effects of the ice protection system and assess how the coatings perform with this system in place, two of the samples which performed best in terms of ice adhesion along with an Aluminium baseline sample were covered in thin wires and then connected to a power supply. The test was conducted in a longer time with an initial 5 min run with no heating at all. Following this, the requisite heating capacity was attained in 5 mins until stabilization at dry conditions. This was followed by the usual 3 min run for ice accretion where the data was logged, and the video captured using the video camera setup. In order to

Table 2
Initial setting for all samples.

Sample	Power setting (W)	Initial Setting
Aluminium	232.7	37.0 V, 6.29 Amps
Wearlon	236.4	38.0 V, 6.22 Amps
TEC- Fsmooth	240.0	37.5 V, 6.40 Amps

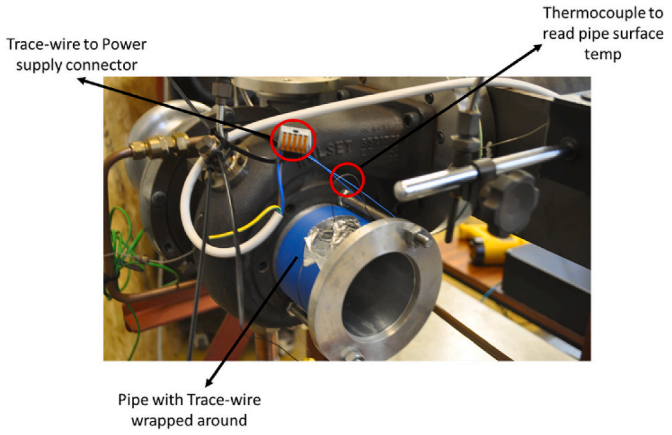

Fig. 9. Trace-wire setup for ice protection effect.

measure the pipe surface temperature, a hole was drilled on the outside of each sample and a thermocouple inserted. Table 2 shows the total power setting for each sample and the initial voltage settings. The setup for the trace-wire tests on the sample pipe in the rig is shown in Fig. 9. Fig. 10 shows the envelope of the trace-wire test run with important phases during the run and significant points marked. (See Table 3.)

4. Results

4.1. Rig test matrix

Two icing conditions were selected based on the most challenging ice accretion to be removed.

The first icing condition, with a turbo rotational speed of 60,000 RPM and an air mass flow of 0.45 kg/s, was selected as it reproduced a heavy accretion of rime ice on the sample due to higher input of injected water (representing a higher level of humidity). This condition was used for visualization of ice accretion within the sample and for characterizing the flow using the High-speed camera and Malvern particle analyser. The turbine exhaust temperature was around −30 °C. Due to the heavy accretion especially around the front and back end of the pipe sample, it was difficult to insert any sort of tool to clear an ice block within the accreted ice and hence this condition was restricted to just visualization and comparison of the potential performance of the various samples.

The second condition, with a turbo rotational speed of 50,000 RPM and an air mass flow of 0.38 kg/s, was selected as it showed a medium yield of rime ice on the sample at a lower level of injected water (representing medium-to-low level of humidity). The condition was used for visualization of ice accretion within the sample, scrape test for determining the ice adhesion strength of the accreted ice, trace-wire tests and for characterizing the flow using the High-speed camera and Malvern particle analyser. The temperature at the exhaust during accretion is around −20 °C. This condition was more stable for the icing rig and resulted in a medium amount of ice accretion on the sample. Due to this, it was easier to insert any cutting tools.

Table 3
Icing rig test matrix.

S. No.	Air Mass Flow (kg/s)	Turbo RPM	Turbine Inlet Absolute Pressure (Bar)	Mixing Ratio (g/kg)	Turbine Exhaust Temperature (°C)	Type of ice expected
1	0.45	60,000	2.5	9	−30	Rime and high-level accretion
2	0.38	50,000	2.0	6.5	−20	Rime and medium level accretion but easier on turbo health and better for scrape test

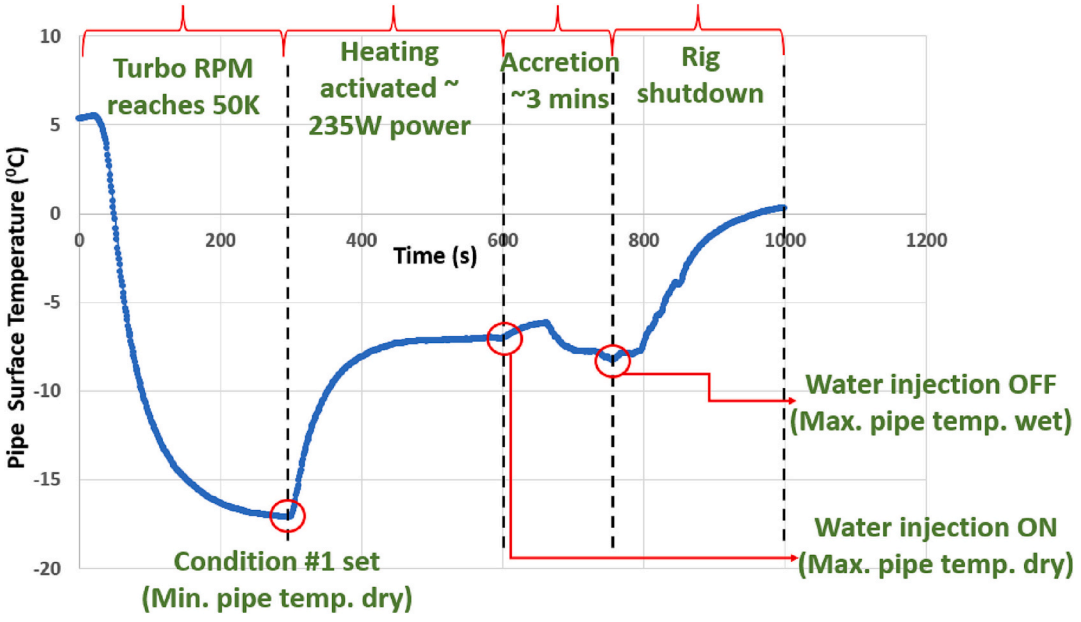

Fig. 10. Envelope of trace-wire test (Time vs Pipe Surface Temperature).

4.2. Ice adhesion test results

There was a total of 8 samples to test with the scrape test setup. The tests were repeated 5 times for each pipe samples to account for statistical variation due to ice being a brittle material. The values for mean adhesion strength and standard deviation have been reported in Table 4. The distribution of shear adhesion obtained from these tests for all samples is plotted in Fig. 11 in a box-and-whiskers plot. The box represents the 25 to 75% quartile of the data set and the median is represented by the line in the box. The whiskers represent the minimum and maximum values in the data set. The 'x' inside the box represents the mean value of the data set.

Fig. 12 shows the reference factor (RF) calculated from the ratio of the mean adhesion strength of the current scroll pipe baseline of Thin SAA + TCS sample (0.65 MPa) with the respective samples as shown in Eq. (3). A RF value above 1 indicates a better performance than the current baseline which is represented in the color green whereas a RF value below 1 indicates worse performance than the current baseline in terms of ice adhesion. The samples performing worse than the current baseline are represented in red.

$$RF = \frac{\tau_{baseline}}{\tau_{sample}} \tag{3}$$

where RF is the reference factor, $\tau_{baseline}$ is the mean value of adhesion strength of the current baseline and τ_{sample} is the mean value of the adhesion strength of the technological sample.

It can be seen from the reference factor calculations in Fig. 12, that Wearlon is the best performing coating and effectively provides better ice adhesion reduction compared to the current baseline Thin SAA + TCS sample. Wearlon is followed by TEC-Fsmooth and TEC-Fthin as the next best coatings in terms of ice adhesion reduction performance. As emphasized by Fig. 11, these 3 coatings were also the one presenting less scatters. On the other hand, Xylan appears to be the worst performing sample. Aluminium was tested as a reference sample and as expected, its performance in term of ice adhesion was significantly worse than Thin SAA + TCS.

No deterioration of the sample coatings could be observed visually or from the results however the process of making slots in the accreted ice did leave some thermal damage marks.

4.3. Ice accretion test results

Ice was accreted on all samples using condition #1 and #2 of the rig test matrix. Thickness measurements were taken at three separate radial points around the region of maximum accretion (mostly at the end of the pipe closer to the turbocharger blades). For both test conditions, the thickness measurements at points of maximum accretion are summarized in Table 5.

For condition #1, Wearlon stands out with extremely low accretion. Thin SAA + TCS had the worst accretion at this condition. TEC-Fsmooth on TSAA also exhibited higher accretion than expected during these tests. As this series of tests has been conducted only once for each sample, a repeat may be necessary to confirm the behaviour of each sample in reducing ice accretion. For condition #2, TEC-Fsmooth exhibits the lowest average ice thickness after 5 runs and Aluminium sample has the maximum average ice thickness. For this condition, the measurements were taken 5 times for each run at three radial locations. The total number of thickness measurements for one sample is 15.

Table 4
Mean adhesion strength and standard deviation for all samples.

Sample	Mean adhesion strength (MPa)	Standard deviation for adhesion strength
Aluminium	0.74	0.241
TEC-Fthin	0.47	0.055
Xylan	0.68	0.198
Thin SAA + PTFE	0.55	0.137
Wearlon	0.29	0.083
TEC-Fsmooth	0.44	0.099
TEC-Fsmooth on TSAA	0.57	0.102
Thin SAA + TCS	0.65	0.181

4.4. Trace-wire test results

For the trace-wire tests, three samples were selected – an aluminium baseline along with the two coatings that performed best in the scrape tests results – Wearlon and TEC-Fsmooth respectively. Condition #2 from the rig test matrix was used for these set of tests and the accretion time was 180 s. With trace-heating, the surface temperature of the sample pipe came closer to −2 to −4 °C at dry conditions. At wet conditions, this temperature went positive (above 0 °C for both Wearlon and TEC-Fsmooth at the interface). Aluminium sample had a lot more accretion towards the bottom of the pipe in the central zone. The ice accreted was quite transparent and less opaque and snow-like compared to the previous tests. The ice detached mid-run for both Wearlon and TEC-Fsmooth. this was found to be a resultant effect of 2 factors: A) the pipe surface temperature going positive and the interface melting; B) and also to a lesser degree, the ice ridge at the back extending into the turbo blades (Fig. 13). Usually, when the ice ridge extends and contacts the turbo blade, only a fraction of ice accreted get delaminated from the pipe surface. But for this instance, with the trace-heating in place, it was observed that the whole ice accretion was removed in one single block and the pipe was completely cleaned out. After shedding, ice accretion started again. Fig. 14 shows the ice which re-accreted in the Wearlon sample.

In summary, it is fair to conclude that with additional heating the two best performing coatings (Wearlon and TEC-Fsmooth) will ease ice shedding from the pipe surface when compared to Aluminium baseline with trace-heating. There was no noticeable damage post the testing on the internal pipe surface specifically from the trace-wire.

Fig. 15 shows the variation of pipe surface temperature over the entire run for all three samples. From this graph, it can be seen that for the dry conditions, the baseline pipe surface temperature without heating is around −15 °C. It is slightly higher for Wearlon, which seems to be due to its insulation capabilities of the coating layer giving a higher reading on the thermocouple compared to the other two samples. The temperature reaches close to −5 °C with the trace-heating settings in place. With the injection of water, the temperature fluctuates and towards the end of run, it goes positive for both Wearlon and TEC-Fsmooth. The Wearlon was observed to have some sort of insulation effect with regards to the ice accretion as the pipe surface temperatures will indicate.

4.5. Characterization of flow results

Using the high-speed camera, a video of the flow is captured for both the test matrix conditions. The total video length is around 1.8 s at 50,000 fps amounting to around 93,000 frames in total. The video for both test matrix conditions was analysed and the size and shape of 100 particles were recorded. The analysis shows that the flow contained mostly spherical or elongated droplets for both test conditions with the occasional irregular shapes. Some of the particles were observed to be solid chunks rather than liquid droplets which could be an indication of the presence of ice crystals in the flow. However, the particles were too small in size to tell conclusively if this is indeed true. Though, it is not an exhaustive analysis of the flow and the particles contained within, it does provide an insight into the characteristics of the flow particles, their shape and size range. The high-speed camera analysis was used primarily to understand the shape of the particles in the flow and whether or not both solid and liquid phases of water were present in the flow. For the statistical analysis, a Malvern particle analyser was used.

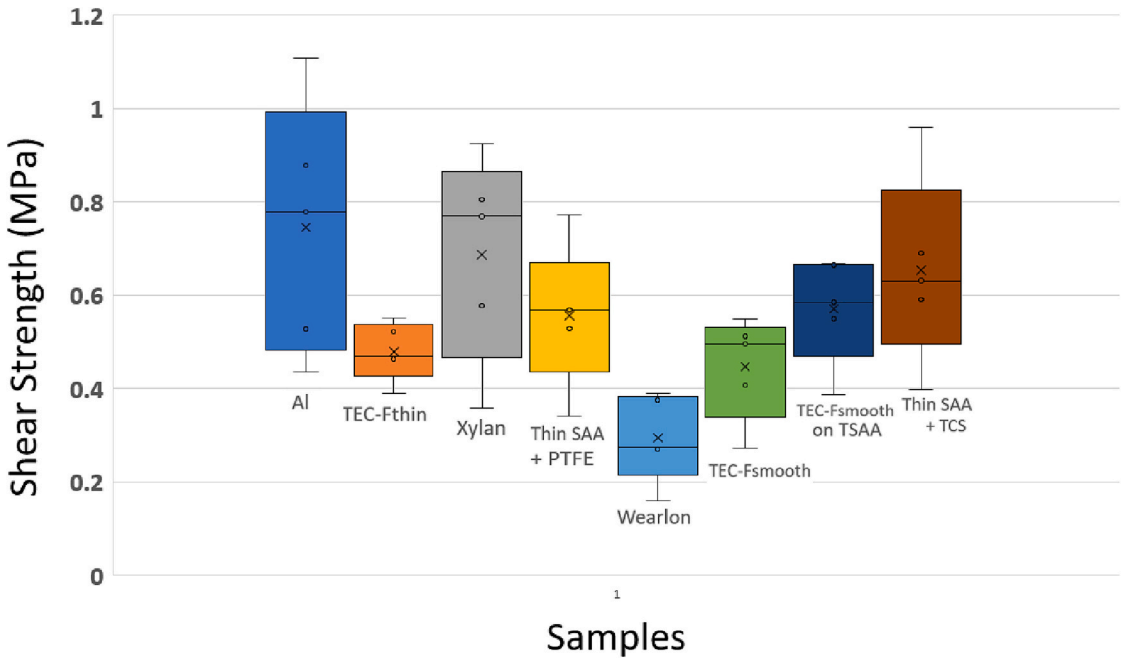

Fig. 11. Shear strength chart for all samples.

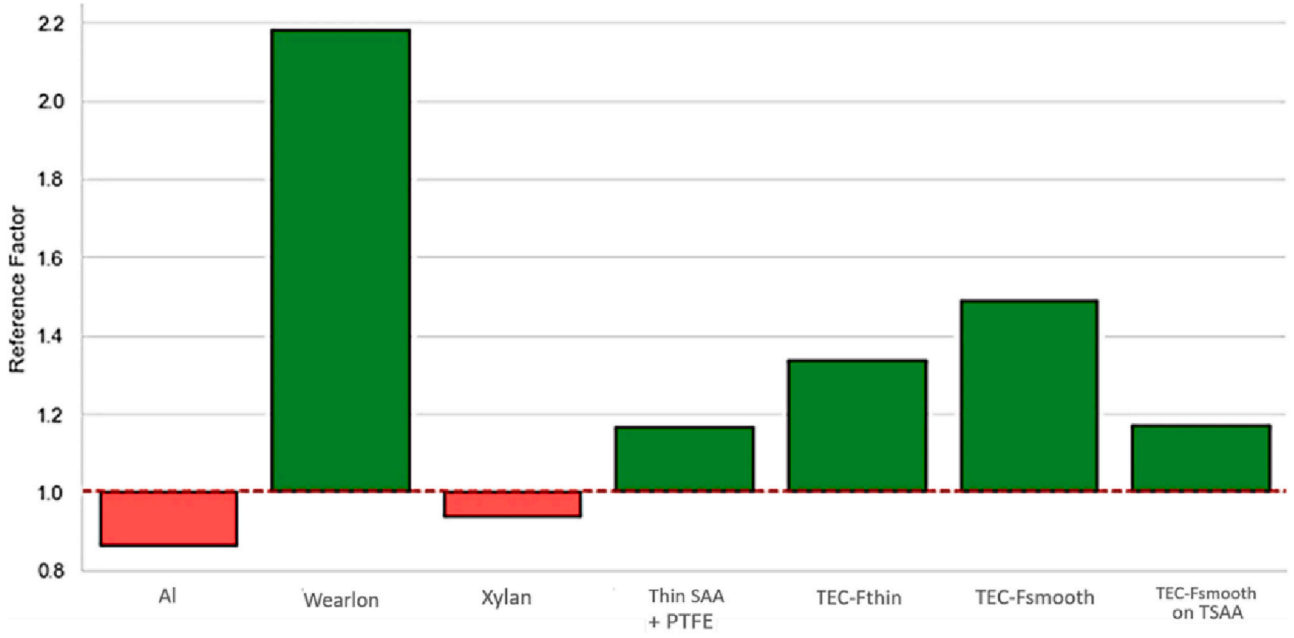

Fig. 12. Reference factor for all samples.

4.5.1. Particle size distribution at test matrix condition #1

The readings were taken over a period of 28 s when the flow was stabilized post reaching the test matrix condition #1. Ice crystals cannot be detected in Malvern, and this is assumed to be one of the main reasons for the unexpected distribution of the particles. From the data collected from the first text matrix condition, the following graph was obtained for the particle size distribution (in μm) over the cumulative volume and volume frequency (both in % as shown in Fig. 16):

The Sauter Mean Diameter or the Surface Area Mean Diameter (D (Clean Sky 2, 2015; Boeing Commercial Aircrafts, 2011)) was found to be around for 29.1 μm whereas the De Brouckere Mean Diameter or Volume Moment Mean Diameter (D (Boeing Commercial Aircrafts, 2011; Kulinich et al., 2009)) which is relevant as it reflects the size of those particles which constitute the bulk of the sample volume was found to be around 205.3 μm for this flow condition. The percentiles for the particle size distribution (Dv10, Dv50 and Dv90) are also reported in Fig. 16.

4.5.2. Particle size distribution at test matrix condition #2

The readings were taken over a period of 33 s when the flow was stabilized post reaching the test matrix condition #2. From the data collected from the second text matrix condition, the following graph was obtained for the particle size distribution (in μm) over the cumulative volume and volume frequency (both in % as shown in Fig. 17):

D (Clean Sky 2, 2015; Boeing Commercial Aircrafts, 2011) was found to be around for 50.49 μm whereas D (Boeing Commercial Aircrafts,

Table 5
Thickness measurements for each sample.

S. No.	Sample	Average ice thickness (mm) - Condition #1 (5 tests per sample)	Ice thickness (mm) - Condition #2 (1 test per sample)
1	Wearlon	11.11	15.64
2	TEC-Fsmooth	17.67	14.05
3	*Al* Sample	19.75	17.98
4	TEC-Fthin	20.68	17.36
5	Thin SAA + TCS	28.95	16.13
6	Thin SAA + PTFE	19.37	15.61
7	Xylan	19.77	16.42
8	TEC-Fsmooth on TSAA	24.23	16.32

2011; Kulinich et al., 2009) was found to be around 249.1 μm for this flow condition. The percentiles for the particle size distribution (Dv10, Dv50 and Dv90) are also reported in Fig. 17.

5. Discussion

This research aimed at developing modern, passive ice protection systems for the air cycle machine exhaust turbine scroll pipe. The final design and construction were able to cover the broad range of icing conditions within the ACM system. There was only a minor issue with pooling of water in the convergent section before the turbocharger turbine inlet in the rig. This delayed the impact of water on the samples thereby delaying the accretion of ice on the samples. The faithful replication of the icing conditions allowed for further investigations with respect to several coatings which were deemed to be prospective future ice protection systems.

5.1. Adhesion test results

The scatter in the adhesion strength results differs greatly for the purely metallic substrate sample of Aluminium 2024-T3 and the other polymeric coatings (commercial or custom-made). This can be due to several reasons that include but are not limited to variability of the test process, thermal gradient effects on different substrates, composition of the surfaces, ice nucleation and growth effects due to material type (Gold, 1970). Given that the test conditions were kept same for each sample and the process was not altered based on sample type, it is reasonable to assume that the main factor for the scatter in the adhesion test results is the properties of the surface itself. The technique for cutting the ice, sample preparation time for scrape test and transfer of the sample to the freezer from the rig can change the internal stresses and play a part in the resulting adhesion strength value. However, since the process was applied consistently for all samples, it still provides a meaningful basis for comparison. Ice nucleation on a surface can be affected by several conditions that include surface properties like geometry, roughness, surface energy etc. The role of hydrophobicity on promoting the ice nucleation delay time is discussed by Oberli et al. (Oberli et al., 2014). As per their research, higher contact angle of droplet on a surface corresponded to higher time delay in ice nucleation. Thus, the characteristics of ice nucleation on the textured hydrophobic surfaces like Wearlon, TEC-Fthin and TEC-Fsmooth etc. is bound to be different from that of the metallic surfaces with the textured surfaces delaying nucleation time. Hydrophilic surfaces like the AA2024-T3 sample have a lower energy barrier for nucleation as compared to hydrophobic textured surfaces, hence leading to a higher nucleation rate of ice (Varanasi et al., 2009). The wettability characteristics of the hydrophilic surfaces like AA2024-T3 sample lead to a higher nucleation rate. This results in a higher amount of nucleation being centred during the early stages of ice formation. Therefore, during the early stages of ice formation, both the rate of ice growth and the thickness of the frost formed are higher on the hydrophilic surfaces as compared to the hydrophobic ones. The dynamic conditions of the rig, however, make the nucleation delaying characteristic of the hydrophobic surfaces tested in this project, into not having a significant impact. This is because the difference in time taken at the beginning of accretion, for the whole surface to be covered by a thin layer of ice observed for the coatings and the Aluminium surface is negligible as observed from the visual recordings.

After the nucleation of ice on a substrate sample, the enthalpy of freezing releases and rapidly increases the local temperature at the ice-

Fig. 13. Ice re-accreted in Wearlon sample during trace-wire tests.

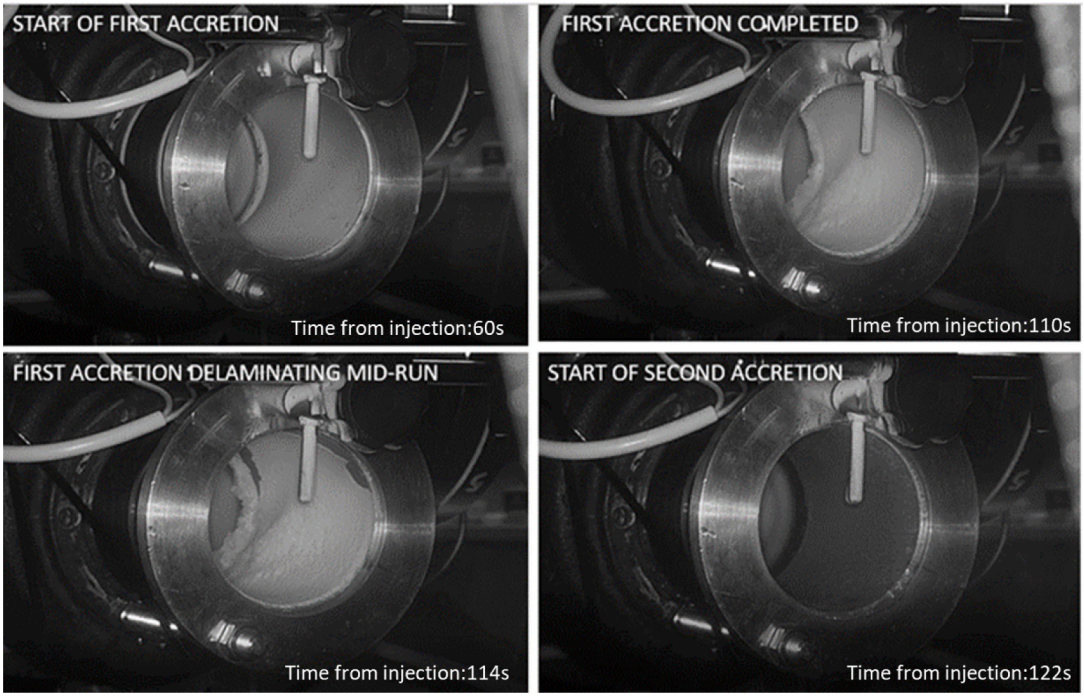

Fig. 14. Accretion run for Wearlon detailing the accretion and delamination.

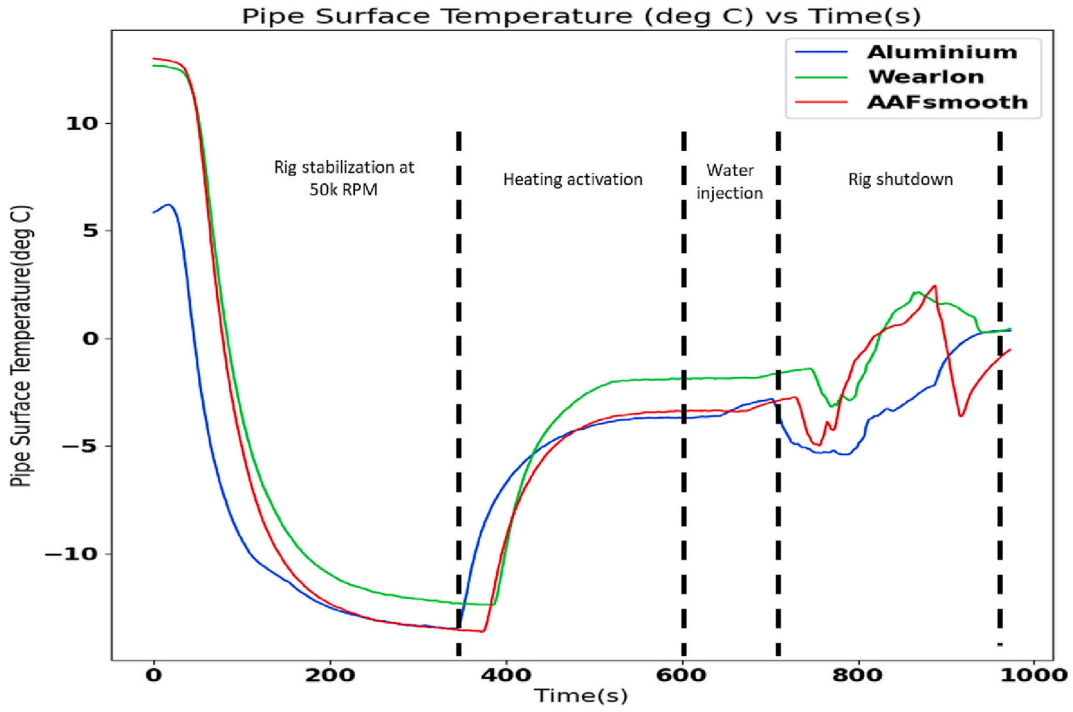

Fig. 15. Time vs Pipe Surface Temperature Chart (all 3 samples).

water interface. The heat transfer from the ice-water interface determines the growth rate of ice phase on a surface (Irajizad et al., 2019). Ice adhesion strength for hydrophobic surfaces is typically low (Irajizad et al., 2019; Fortin, 2017) and this is confirmed by the testing. The scatter within the adhesion values is also found to be lower for some of the surfaces like TEC-Fthin, Wearlon and TEC-Fsmooth when compared to the metallic surface of AA2024-T3 sample. This can be assumed to be a feature of the composition of the surface and its particular texturing. The number of test runs done on the samples can also be a determining factor as more tests may have resulted in the eventual degradation of the textured surfaces resulting in possible higher adhesion strength values and higher scatter for some of the samples. Xylan appears to be the only hydrophobic coating sample that showed unexpected results both in terms of adhesive strength and scatter and even appears to perform worse than the current baseline and further investigation of its material properties is required to explain this anomalous behaviour which was not possible due to the proprietary nature of the coating.

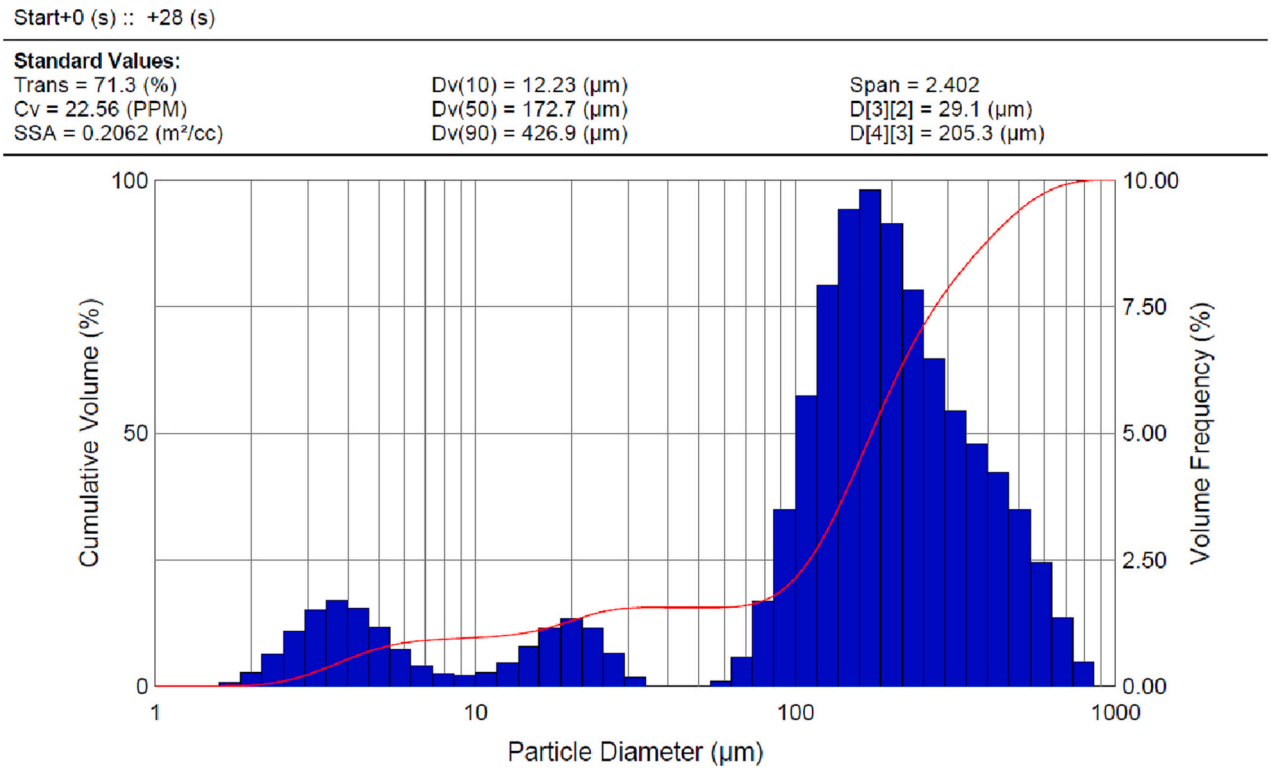

Fig. 16. Averaged Particle Size Distribution at Test matrix Condition #1.

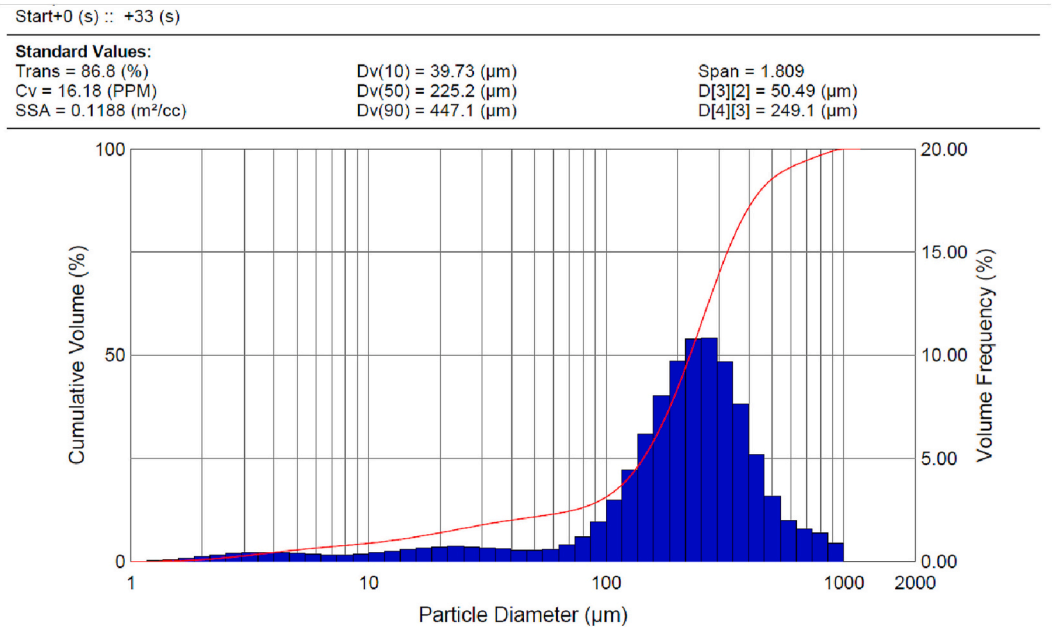

Fig. 17. Averaged Particle Size Distribution for test matrix condition #2.

5.2. *Future development in ice protection systems*

Prospective candidate coatings which could be used as passive ice protection solutions were tested as part of this research work. These coatings were deposited on the baseline samples and ice was accreted on them. This accreted ice was then tested using a new shear adhesion test method. The coatings were designed to be hydrophobic with very low surface free energy. However, as seen from the literature review, even more advanced materials like superhydrophobic and icephobic materials can turn into surfaces that promote ice accretion under dynamic icing conditions. These conditions were present in the rig and will also be present in the actual turbomachinery. This currently means that a great level of refinement needs to be attained in both development of modern coatings which can be used as future ice protection systems.

As noted by Jung et al. (Jung et al., 2012), the icephobicity of a surface is very much dependent on the environmental factors it is under. The effectiveness of the hydrophobic, superhydrophobic and icephobic surfaces can be reduced greatly under certain dynamic conditions since

the nucleation of water into ice can occur through the homogeneous mechanism (from the liquid-gas or liquid-liquid interface) rather than the usual heterogeneous mechanism (liquid-solid interface). A similar observation was made in the testing done for ERICE project where hydrophobic coatings, both commercial and custom-made, accreted ice under the conditions developed within the rig, but which mechanism led to this is still not clear and requires more in-depth study. The two best coatings found with the testing conducted as part of this research work still accreted a significant amount of ice as shown in Fig. 18.

However, it is important to note that the specially textured and custom-made materials did show better performance than the current baseline. This means that these candidate coatings still reduce the interfacial adhesion relative to the current standard used within the ACM system even if they do not resist ice accretion effectively. Ice accretion is really difficult to engineer against, especially when the conditions are so dynamic as they are in the ACM turbine scroll pipe. This mainly due to multiple factors like impurities, extremely low temperatures, pre-wetting of the accretion surface and the material characteristics of the surface itself. Presence of a liquid-layer atop the substrate can aid in accretion of ice as noted by (Jung et al., 2012). This is usually the case when dynamic conditions like those within ACM are present which may further degrade the performance of any possible candidates for passive ice protection.

Another interesting observation from the testing was the performance of the coatings with the trace-wire system. The tests revealed that the two best performing coatings i.e., Wearlon and TEC-Fsmooth actually shed the accreted ice with ease when the pipe surface was heated. This system is close to the actual ice protection system present in the ACM system known as a “hot-lip” system. Additional testing and validation will be required with the actual turbomachinery, however, there is a good indication that the most effective coatings might reduce the current power consumption levels from the ACM ice protection system. This contributes directly towards the Clean Sky 2 goals of moving towards an eco-friendlier aircraft (Clean Sky 2, 2015). The joint technical programme lays out the requirements for aircraft systems for the future to be more optimized with direct contributions to environmental objectives that result in decrease in fuel consumption, reduce emissions and help in enabling more bleed-less systems. Using the coatings in conjunction with the ice protection system helps in achieving these targets and provides a platform for the development of better systems in the future.

This also however indicates that current hydrophobic surfaces, even those engineered specifically to have low surface free energy, are not ready to be deployed as sole countermeasures against icing, especially in aviation. They need to be developed further in order to have the required level of performance that satisfies the operational safety targets specified for ice protection equipment on commercial aircrafts described in CS-25 Subpart F ((EASA), European Aviation Safety Agency, 2021).

6. Conclusions

An icing rig was developed along with a new shear adhesion testing technique for ice accreted within an ACM turbine scroll pipe. The rig was able to successfully replicate the icing conditions observed within the ACM system which forms part of the air conditioning packs within the aircraft. Six prospective candidate coatings which were considered to be viable solutions as passive ice protection systems were tested using this rig setup along with the current baseline of Thin SAA + TCS and an Aluminium alloy sample. The coatings were accreted with ice at two different test matrix conditions. The accreted ice from one of the test matrix conditions was tested using the Scrape test setup and the shear adhesion strength values were noted. The testing revealed that Wearlon and TEC-Fsmooth were the best performing coatings and except for Xylan and basic Aluminium AA2024-T3 alloy pipe, all other samples performed better than the current standard baseline of Thin SAA + TCS.

A first characterization of the outlet flow of the ACM in icing conditions has been reported. This flow was characterized using a highspeed camera and a Malvern particle analyser which helped in identifying the droplet sizes and particle distribution for the ACM icing conditions. The high-speed camera results indicated the possible presence of ice particles in the flow, amongst super-cooled liquid droplets. The Malvern testing indicates presence of particle sizes over 200 μm in the flow for both test matrix conditions with the higher particle size present for the second test matrix condition which is closer to 250 μm.

The ice protection, hot-lip system currently existing in ACM systems was replicated with a trace-wire test setup on two of the best candidate

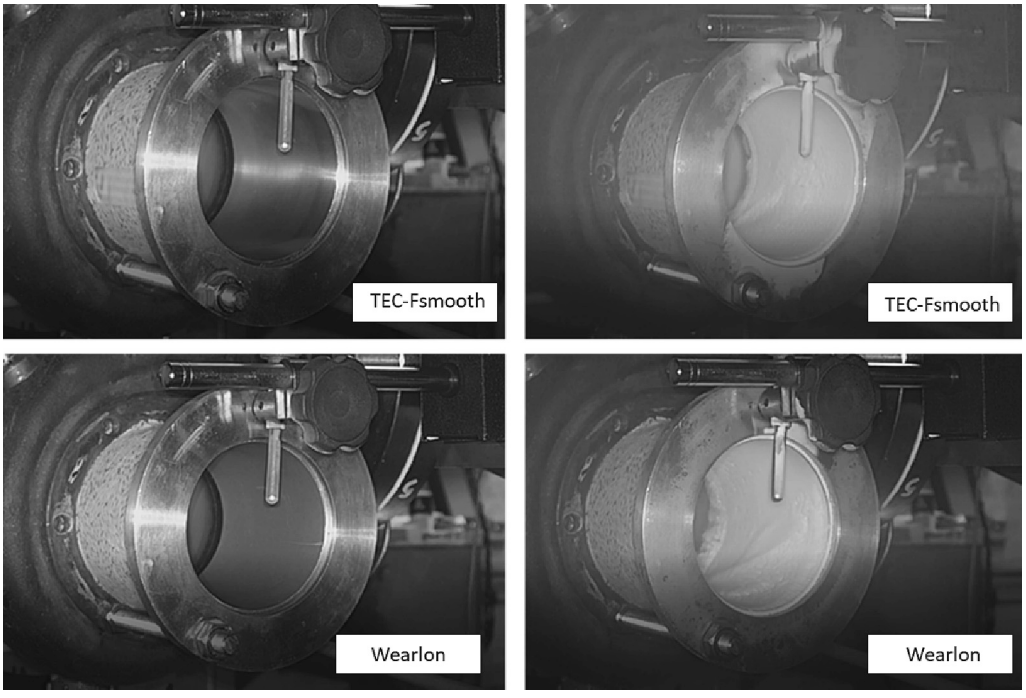

Fig. 18. TEC-Fsmooth and Wearlon samples before and after subject to testing conditions.

coatings. Both coatings expedite the shedding of ice on the scroll pipe. This testing confirms that based on the current performance of the passive ice protection solutions tested in this research work, a hybrid system consisting of the active hot-lip system and the coatings is the best path forward to reduce energy consumption and maintain de-icing performance at the required levels.

CRediT authorship contribution statement

A. Vincent: Conceptualization, Methodology, Investigation, Formal analysis, Software, Writing – original draft. **M.L.A. Pervier:** Conceptualization, Supervision, Writing – review & editing, Funding acquisition. **H. Pervier:** Conceptualization, Methodology, Funding acquisition. **D. Nalianda:** Supervision, Writing – review & editing. **P. West:** Investigation, Validation. **C. Agustin-Saenz:** Conceptualization, Methodology. **F. Brusciotti:** Conceptualization, Writing – review & editing, Project administration, Funding acquisition.

Declaration of Competing Interest

None.

Data availability

Data will be made available on request.

Acknowledgement

This research was funded from the Clean Sky 2 Joint Undertaking (CSJU) under grant agreement No. 821301. The JU received support from the European Union's Horizon 2020 (H2020) research and innovation programme and the Clean Sky 2 JU members other than the Union.

Appendix A. Supplementary data

Supplementary data to this article can be found online at https://doi.org/10.1016/j.coldregions.2023.103912.

References

(EASA), European Aviation Safety Agency, 2021. CS-25 Certification Specifications and Acceptable Means of Compliance for Large Aeroplanes. EASA.
An, F., Vincent, A., Pervier, M., 2022. Measurement and FEM of ice adhesion to the downstream pipe of an air cycle machine. Cold Reg. Sci. Technol. 196.
Andenæs, E., Jellea, B.P., Ramloa, K., Kolås, T., Seljd, J., Foss, S.E., 2018. The influence of snow and ice coverage on the energy generation from photovoltaic solar cells. Sol. Energy 159, 318–328.
Beeram, P., Waldman, R., Hu, H., 2017. Ice adhesion measurements of ice mitigation coatings pertinent to aircraft icing. In: 9th AIAA Atmospheric and Space Environments Conference, Denver, Colorado.
Boeing Commercial Aircrafts, 2011. Commercial Airliner Environmental Control System: Engineering Aspects of Cabin Air Quality. Boeing Co., Renton, Washington.
Clean Sky 2, 2015. Clean Sky 2 Joint Technical Programme, 23 May. [Online]. Available. https://ec.europa.eu/research/participants/data/ref/h2020/other/guide-appl/jti/h2020-guide-techprog-cleansky-ju_en.pdf [Accessed 14 Jan 2019].
Fortin, G., 2017. Super-Hydrophobic Coatings as a Part of the Aircraft Ice Protection System. SAE International.
Gao, L., Hu, H., 2021. Wind turbine icing characteristics and icing-induced power losses to utility-scale wind turbines. PNAS 118 (42).
Gold, L., 1970. Process of failure in ice. Can. Geotech. J. 7 (4), 405–413.
Grosshans, H., 2012. Evaporation of a Droplet. Lund University, Lund, Sweden.
Irajizad, P., Nazifi, S., Ghasemi, H., 2019. Icephobic surfaces: definition and figures of merit. Adv. Colloid Interf. Sci. 269, 203–218.
Jung, S., Tiwari, M.K., Doan, N.V., Poulikakos, D., 2012. Mechanism of Supercooled Droplet Freezing on Surfaces. Nature Communications, Zurich, Switzerland.
Kool, N., Orchard, D., Chevrette, G., 2018. Testing of Elastomer Icephobic Coatings. AIAA, Atlanta, US.
Kulinich, S., Farzaneh, M., Farhadi, S., 2009. Ice Adhesion on Superhydrophobic and Hydrophobic Surfaces: Effect of Wetting Hysteresis. IWAIS, Quebec, CA.
Laforte, C., Blackburn, C., Perron, J., 2015. A Review of Icephobic Coating Performances over the Last Decade. SAE International, Quebec, Canada.
Oberli, L., Caruso, D., Hall, C., Fabretto, M., Murphy, P., Evans, D., 2014. Condensation and freezing of droplets on superhydrophobic surfaces. Adv. Colloid Interf. Sci. 210, 47–57.
Pervier, M.-L., 2012. Mechanics of Ice Detachment Applied to Turbomachinery. Cranfield University, Cranfield.
Ryerson, C.C., 2011. Ice protection of offshore platforms. Cold Reg. Sci. Technol. 65 (1), 97–110.
SD, G., 2006. A study of U.S. inflight icing accidents and incidents, 1978 to 2002. In: 44th AIAA Aerospace Sciences Meeting and Exhibit.
Experimental results on the tensile strength of atmospheric ice. Trans. Can. Soc. Mech. Eng. 13 (3), 1989, 59–64.
Varanasi, K.K., Hsu, M., Bhate, N., Yang, W., Deng, T., 2009. Spatial control in the heterogeneous nucleation of water. Appl. Phys. Lett. 95.
Xiao, S., He, J., Zhang, Z., 2017. Modeling nanoscale ice adhesion. Acta Mech. Solid Sin. 30 (3), 224–236.

https://dspace.org/

Experimental rig for ice accretion and adhesion strength measurement for air cycle machine system

Vincent, Abhay; Pervier, Marie Laure A.; Pervier, Hugo; Nalianda, Devaiah; West, Peter ...

2023-09-01
Elsevier
https://doi.org/10.1016/j.coldregions.2023.103912
Vincent A, Pervier MLA, Pervier H, et al., (2023) Experimental rig for ice accretion and adhesion strength measurement for air cycle machine system. Cold Regions Science and Technology, Volume 213, September 2023, Article Number 103912

Downloaded from a DSpace repository. https://dspace.org/